Water Supply

Water Supply Vol 22 No 3, 2659 doi: 10.2166/ws.2021.446

Experimental study on flow over arced-plan porous weirs

M. Pirzad, M. H. Pourmohammadi*, H. Ghorbanizadeh Kharazi, M. Solimani Babarsad and E. Derikvand

Department of Civil Engineering, Water Resources Engineering and Management, Shoushtar Branch, Islamic Azad University, Shoushtar, Iran
*Corresponding author. E-mail: purmohammadi@gmail.com

MS, 0000-0002-6676-0323

ABSTRACT

Unlike conventional impermeable weirs, porous weirs do not clog the flow and passage of aquatic life with increased aeration or aerobic reactions. They have minimal negative effects on the environment and are known as environmentally friendly structures. This study experimentally investigates the hydraulic performance of arced-plan porous weirs (APPWs) in different hydraulic and geometric conditions. For this purpose, four different porous and two solid weirs were examined. Experiments were conducted in a horizontal laboratory flume with length, width and height of 20, 0.6 and 0.5 m, respectively, for a wide range of flow rates, particle sizes and three arc lengths. Results showed that increasing filling material sizes increases the free discharge coefficient and reduces the submerged discharge reduction factor (DRF). It was also concluded that the weirs' effective length significantly impacts the free discharge coefficient and has no significant effect on the threshold submergence index and submerged DRF. Unlike solid weirs, the threshold submergence of porous weirs occurs at a downstream depth lower than the weir's height. Finally, according to the dimensional analysis and gene-expression programming approach, three relations were extracted to calculate the free discharge coefficient, threshold submergence index and submerged DRF for APPWs.

Key words: arced-plan porous weir, discharge coefficient, discharge reduction factor, gene-expression programming, threshold submergence index

HIGHLIGHTS

- Analyze the hydraulic performance of the arced-plan porous weirs for different hydraulic and geometrical conditions.
- Determine the boundary between modular and non-modular flow.
- Develop new equations for discharge coefficient in free flow, modular limit index and discharge reduction factor in submerged flow.
- Investigate the effect of weir direction on the hydraulic performance of arced-plan porous weirs.

INTRODUCTION

Hydraulic structures made of metal mesh and stone have been used in various fields of water engineering, such as stepped spillways for energy dissipation, groins for bed and riverbank erosion control, and detention dams for flood control. In the last decade, engineers have tried to change nature and landscapes as little as possible alongside construction. Rigid concrete structures disrupt aquatic traffic, especially in rivers and natural canals, and negatively affect the environment and natural landscapes.

Weirs are usually made of impermeable materials such as concrete. These impermeable bodies prevent the longitudinal movement of aquatic organisms, and physical and chemical substances in the water, and as a result, cause accumulation of sediment behind the weir and negative effects on the water ecosystem (Mohamed 2010). Researchers have recently tried to use inexpensive and available natural materials to eliminate these destructive effects and not change the natural landscape. Among these, porous weirs with characteristics such as stability (no pressure and low boiling force), economic efficiency (use of available and natural materials), permeability and flexibility against forces are good alternatives (Fathi-moghadam *et al.* 2018; Rahmanshahi & Shafai Bejestan 2020). According to Chanson (2006), these structures are among the recommended and valuable structures for future studies. These types of structures with more aeration cause the activity of aerobic microorganisms and thus increase the self-purification capacity of the river. Increasing the self-

purification capacity will purify water and eliminate bad odours in waterways to which sewage is discharged (Mohamed 2010; Fathi-moghadam *et al.* 2018).

So far, several studies have been conducted on the flow inside the permeable bodies. However, in most of these studies, the upstream depth is less than the height of its crest, and the interaction between the over and through flows and their effects on each other has been less considered. Kells (1993) studied the gradual variable flow over the gravel dam for two different flow conditions, including partial and complete fall from the dam. Kells (1994) showed that the ratio of through flow to overflow in the gravel dam ranges from 0.25 to 0.5. Michioku *et al.* (2005) studied the hydrodynamics of a rubble mound theoretically and experimentally. Performing a one-dimensional analysis on a constant uniform flow through the rubble mound, they described that the discharge is a function of parameters such as upstream and downstream flow depth, porosity, gravel particle diameter and rubble mound length. Michioku *et al.* (2007) conducted laboratory studies on flow over weirs and gravel groins. Their findings showed the mass and momentum changes between the mainstream and the stream in the porous media. Leu *et al.* (2008) studied turbulent flow around a permeable body. They examined three models with porosities of 0, 34.9, and 47.5% and showed that the downstream rotation area is larger for porous structures due to the passage of flow through it.

Mohamed (2010) investigated two models of rectangular gabion weirs and two solid weirs with the same geometry for comparison and provided two relationships for predicting the discharge coefficient in free and submerged flow conditions. Salmasi & Taghi Sattari (2017) experimentally studied the hydraulic performance of broad-crested gabion weirs in free and submerged flow conditions. Finally, using the M5 model, they extracted relationships for the discharge coefficient in both conditions. Mohammadpour *et al.* (2013) numerically modelled the flow on the porous broad-crested weirs. Their results showed that the k-ε model has better accuracy for modelling this type of weir. Fathi-moghadam *et al.* (2018), using the Flow3D numerical model, investigated the flow pattern and the hydraulic performance of porous trapezoidal and triangular weirs in free-flow conditions. The study also discussed energy dissipation and over and through flow rates. Safarzadeh & Mohajeri (2018) numerically simulated broad-crested weirs in free-flow conditions and provided relationships to calculate the discharge coefficient. The ratio of through flow to total flow in different hydraulic and geometric conditions was obtained in this research. Also, new relationships were extracted to calculate the discharge coefficient using a nonlinear multivariate regression model. Salmasi & Taghi Sattari (2017) and Salmasi *et al.* (2021) experimentally investigated the hydraulic performance of porous broad-crested weirs under free and submerged flow conditions with four different porosities. Their results indicated that the discharge coefficient in submerged flow is approximately 20% lower than the free-flow discharge coefficient. Shariq *et al.* (2020) investigated the porous broad-crested weir discharge equation under through flow conditions. Their results reveal that the discharge through the porous broad-crested weir is more sensitive to the material size and upstream depth than the downstream depth of the porous broad-crested weir.

According to the common weir's head-discharge relationship ($Q = C_d W \sqrt{2g} H^{1.5}$) (Fritz & Hager 1998), to increase the hydraulic performance of the weirs, the discharge coefficient or the effective length of the weir can be increased (Crookston & Tullis 2012). So far, various works have been done in this field in impermeable weirs. Using an arced-plan and a W-shape or zigzag increases the effective length of the weir and increases its performance. The main idea of this research was that a porous weir with an arced-plan increases flow rate, first because it is porous (because it has both through and overflow), and second, the arc plan increases the effective length of the weir. According to the research background, previous studies regarding permeable weirs were mainly involved with linear-plan broad-crested weirs. Thus, no comprehensive research has been conducted on the hydraulic performance of arced-plan porous weir (APPWs) in free and submerged flow conditions. In addition, none of the previous studies examined the threshold of submergence or the modular limit of porous weirs. Thus, there is a lack of comprehensive research on the hydraulics of such weirs.

The main purpose of this study is to investigate the hydraulic performance of the APPW experimentally. For this purpose, experiments were conducted on different physical models of APPWs to determine the effect of various factors such as flow rate, material size and geometrical dimensions of weirs on their free discharge coefficient, threshold submergence and submerged discharge reduction factor (DRF). The performance of two porous weirs was also compared to their corresponding solid weirs. In addition, two weirs with the same geometry but with different directions were tested to investigate the effect of the arced-plan weir direction on its hydraulic performance in free and submerged conditions. Finally, the gene-expression programming (GEP) approach with multivariable nonlinear regression was used to develop three mathematical equations for free discharge coefficient, threshold submergence index and submerged DRF for engineers to use in APPW design.

MATERIAL AND METHODS

Experimental setup and measurements

The experiments of this research were performed in a horizontal, glass-walled laboratory flume with length, width and height of 20, 0.6 and 0.5 m, respectively, in Khuzestan Water and Power Authority (KWPA) laboratory, Iran. The flume has a closed water flow system, and an end gate was used to control the downstream depth in submerged flow conditions. A rectangular weir at the downstream end of the system was used to measure the discharge, and a point gauge with an accuracy of ± 0.2 mm was used to measure water surface elevation. The weirs were made of a metal rod with a diameter of 4 mm and covered with 5×5 mm fine wire mesh, smaller than the smallest filling stones. The model frames were filled with different gravel sizes with a coefficient of uniformity of the materials near 1. There are five sizes of filling material used in porous weirs, with almost uniform diameters of 7.13–31.75 mm and sharp corners. In this research, four porous and two solid weirs were constructed. Two solid weirs corresponded to PW-M1 and PW-M3 and were made of plexiglas. They were compared to the corresponding porous weirs. The physical model test matrix also included one APPW weir with inverted direction. This experiment was performed to investigate the directional effect of APPW.

It is not always practical to set the weir in only free-flow conditions or to avoid submergence. On the other hand, the performance of the control flow structure depends mainly on the downstream water level; hence, all experiments were carried out for free and submerged flow conditions to understand better the effect of the flow status on the hydraulic behaviour of flow over and through the porous weirs. In addition, the threshold submergence is determined as the water level boundary in which the free approach flow regime turns into submergence. This is defined as the water level where the upstream water depth starts to increase by +1 mm due to the increase of downstream water depth (Hager & Schwalt 1994; Fritz & Hager 1998).

In free condition experiments, after stabilizing the flow discharge and the upstream head over the weir, the upstream water depth was measured at a distance about four times the head over the weir. To determine the threshold submergence boundary, the downstream water depth was slowly increased using the end gate until the upstream flow depth was increased by 1 mm. Then, using up and downstream water depths, the threshold submergence index was calculated. This procedure was continued for various submergence ratios to calculate the submerged DRF. All measurements were made along the centreline of the flume.

Figure 1 shows definition sketches and experimental views of porous and solid weirs used in this study. Geometric details and acronyms for the constructed models are given in Table 1. In Table 1, PW refers to a porous weir, IPW refers to the inverted porous weir and SW refers to a solid weir. Also, L_c is the length of the weir crest, P is weir height, Q is flow discharge, W is channel width, d_{50} is gravel median size, n is gravel porosity, and L_{arc} is weir's effective length. In this research, all models were tested in different discharges, and a total of 175, 175 and 1,708 experiments were performed in free, threshold submergence and submerged flow conditions, respectively.

Dimensional analysis of APPW

Free discharge coefficient, C_d and flow rate are calculated in Equation (1) (Fritz & Hager 1998):

$$Q = C_d W \sqrt{2g} H^{1.5} \tag{1}$$

where Q is water discharge, W is the width of the weir, g is the gravitational acceleration, H is the total upstream head ($H = h + v^2/2g$), h is the head over the weir and v is the approach velocity.

For an APPW, the discharge coefficient can be expressed by the following functional relationship:

$$f(C_d,\ h,\ L_c, P,\ Q,\ g,\ \sigma,\ \rho,\ \mu,\ d_{50},\ n,\ L_{Arc}) = 0 \tag{2}$$

in which f is a functional symbol, σ is surface tension, ρ is water density, μ is water viscosity, h is upstream water level and n is gravel porosity.

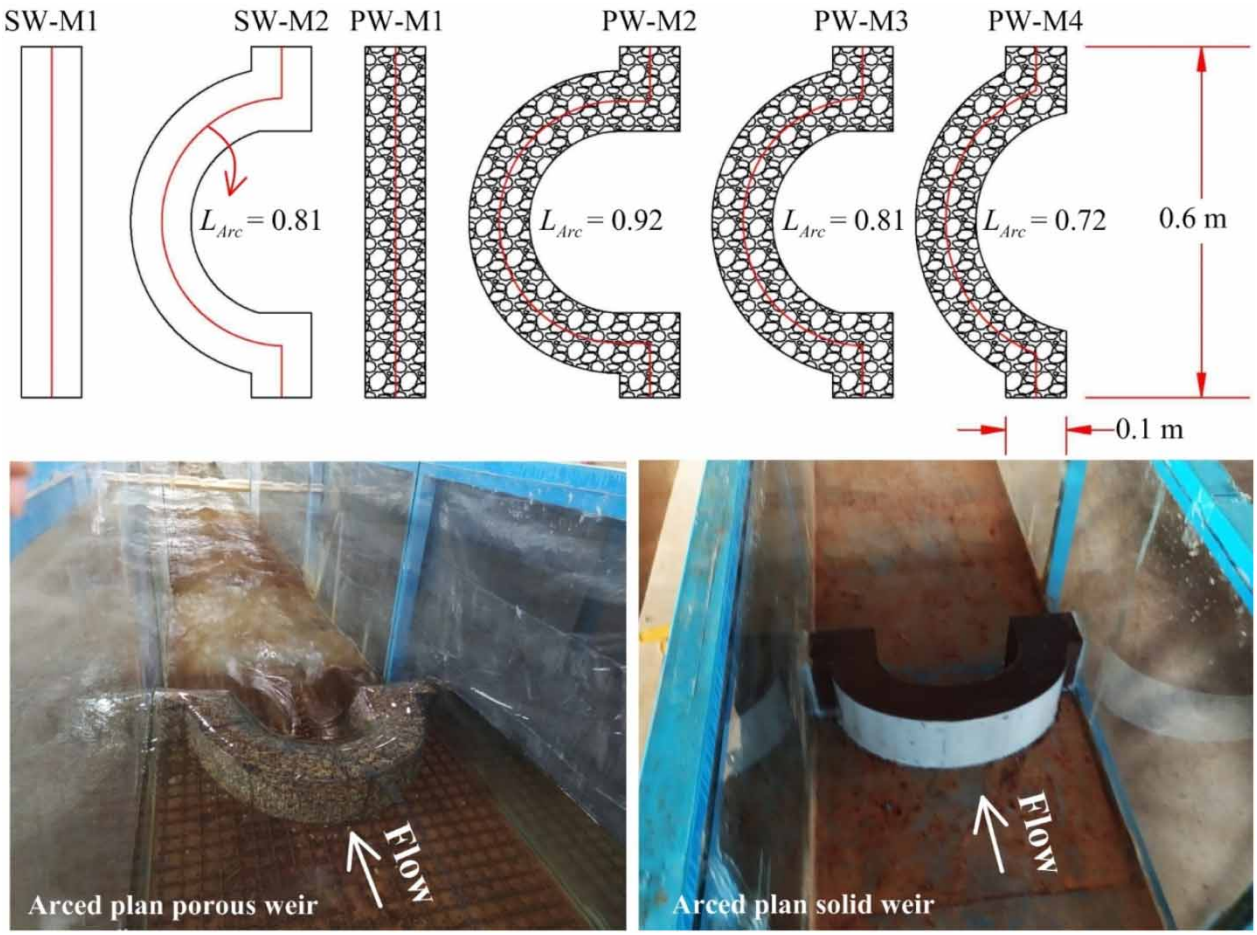

Figure 1 | Definition sketches and experimental views of arced-plan porous and solid weirs.

Table 1 | Experimental models variables

Model name	L_c (m)	P (m)	W (m)	Q (l/s)	L_{Arc} (cm)	d_{50} (mm)	n (%)
PW-M1	0.1	0.16	0.6	10.36–64.88	60	7.13, 11.10, 15.87, 22.22, 31.75	54, 46, 44, 47, 56
PW-M2				14.80–64.25	92.13		
PW-M3				14.80–64.25	81.45		
PW-M4				10.36–64.88	71.97		
IPW-M3	0.1	0.16	0.6	15.44–64.88	81.45	15.87	44
SW-M1	0.1	0.16	0.6	7.19–64.88	60	–	–
SW-M2				3.39–64.88	81.45		

Using the Π theorem of dimensional analysis (Barenblatt 1987) for the parameters in Equation (2), C_d can be expressed by following dimensionless groups:

$$C_d = f(H/P,\ L_c/L_{Arc},\ Re,\ d_{50}/P,\ n,\ We) \tag{3}$$

where Re = Reynolds number and We = Weber number.

At a specified boundary of the downstream depth, h_{TS}, the weir's upstream depth begins to increase as the depth increases. This boundary is known as the threshold submergence. For porous weirs, the threshold submergence index can be explained as $Y_{TS} = (h_{TS} - P)/P$. Similar to free-flow conditions, by applying the dimensional analysis, the threshold submergence index can be formulated as:

$$Y_{TS} = f(H/P,\ L_c/L_{Arc}, Re,\ d_{50}/P,\ n,\ We) \tag{4}$$

Generally, for a specified weir's upstream head, the submerged discharge, Q_s, is smaller than that in the free-flow condition, Q. Hence, the discharge for the submerged flow is defined by the following equation:

$$Q_s = \mathrm{DRF} \times Q \ \rightarrow \ \mathrm{DRF} = \frac{Q_s}{Q} \tag{5}$$

In addition to the governing parameters in free-flow conditions, the downstream depth, h_d, affects the DRF. In this study, DRF can be described by the following functional relationship:

$$\mathrm{DRF} = f(\Gamma,\ L_c/L_{Arc}, Re,\ d_{50}/P,\ n,\ We) \tag{6}$$

where $\Gamma = ((h_d/h_u) - (h_{TS}/h_u))/(1 - (h_{TS}/h_u))$ (h_u = upstream depth) is defined as the submergence index, which for free flow $\Gamma < 0$ (indicating that the weir is not submerged), for modular limit $\Gamma = 0$, and for fully submerged flow condition $\Gamma = 1$.

In all experiments, the head over the weirs was larger than 3 cm to eliminate the effect of surface tension and the Weber number from Equations (3), (4) and (6) (Horton 1907; Novak & Cabelka 1981). According to Table 2, the Reynolds number in all experiments was high enough to provide a fully turbulent flow and was not taken into account. The ranges of effective independent variables in Equations (3), (4) and (6) based on experimental data are given in Table 2. Consequently, three functional relationships are simplified as follows:

$$C_d = f(H/P,\ L_c/L_{Arc}, d_{50}/P,\ n) \tag{7}$$

$$Y_{TS} = f(H/P,\ L_c/L_{Arc}, d_{50}/P,\ n) \tag{8}$$

$$\mathrm{DRF} = f(\Gamma, L_c/L_{Arc}, d_{50}/P,\ n) \tag{9}$$

RESULTS AND DISCUSSIONS

The flow over weirs can be modular or non-modular. Figure 2 shows the modular or free-flow condition on PW-M3. The water surface profile downstream of the arced-plan weirs in free-flow conditions has a convexity in the channel's centreline that increases with increasing flow rate. Figure 2(b) illustrates the non-modular or submerged flow condition over SW-M2. Like other type of weirs, the weir's downstream water surface in the submerged conditions has surface waves that decrease with increasing submergence ratio.

Figure 3 depicts the discharge coefficient for PW-M1 and PW-M2 at the different flow rates in free and submerged flow conditions. Clearly, with the increase of weirs submergence, the discharge coefficient decreases, and according to Equation (5), the submerged discharge coefficient is a reduction coefficient in a free condition. The results also show that in low flow rates, the discharge coefficient decreases at a higher rate. According to these figures, the submerged discharge coefficient can be 68% less than the corresponding free-flow discharge coefficient.

Table 2 | Range of independent dimensionless variables

	Independent dimensionless variables					
Range	H/P	Γ	L_c/L_{Arc}	$Re \times 10^{-4}$	n	d_{50}/P
Min	0.153	0	0.108	1.75	0.44	0.045
Max	0.89	1	0.167	10.94	0.56	0.198

Figure 2 | Water surface profile in (a) free and (b) submerged flow conditions over PW-M3 and SW-M2 models, respectively.

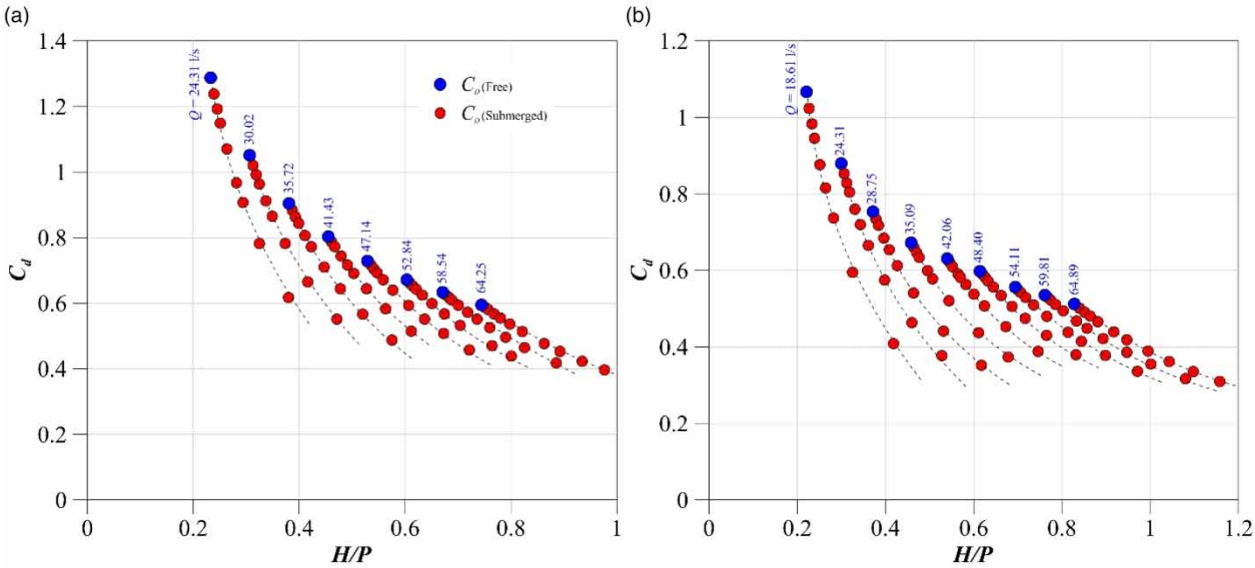

Figure 3 | Discharge coefficient versus *H/P* for free and submerged flow conditions of (a) PW-M1 and (b) PW-M2.

Free-flow condition

The free conditions discharge coefficients are calculated using Equation (1). Figure 4 shows the discharge coefficient versus H/P for PW-M1 and PW-M3 for all values of d_{50}/P (the ratio of the mean size of filling materials to the weir's height). The discharge coefficient of the two corresponding solid weirs (SW-M1 and SW-M2) is also presented for comparison with the porous weir. Results show that with increasing material sizes, the discharge coefficient increases. Also, experimental observation indicated that increasing particle sizes reduces the upstream water level due to increased pores size. According to the Darcy–Weisbach equation, as the size of the weir's filling material increases, the pore diameter increases, and the through-flow resistance decreases. Due to the lower flow resistance in porous weirs, the through-flow fraction and the discharge coefficient increase. Unlike porous weirs, the discharge coefficient increases with increasing H/P (or discharge) ratio in solid weirs and becomes almost constant for $H/P > 0.8$. Results show that the difference between C_d of different particle sizes is reduced with increasing H/P. This is a direct consequence of the reduced ratio of through-flow to total flow discharge. For H/P values greater than 0.9, the discharge coefficient values of solid and porous weirs are very close to each other.

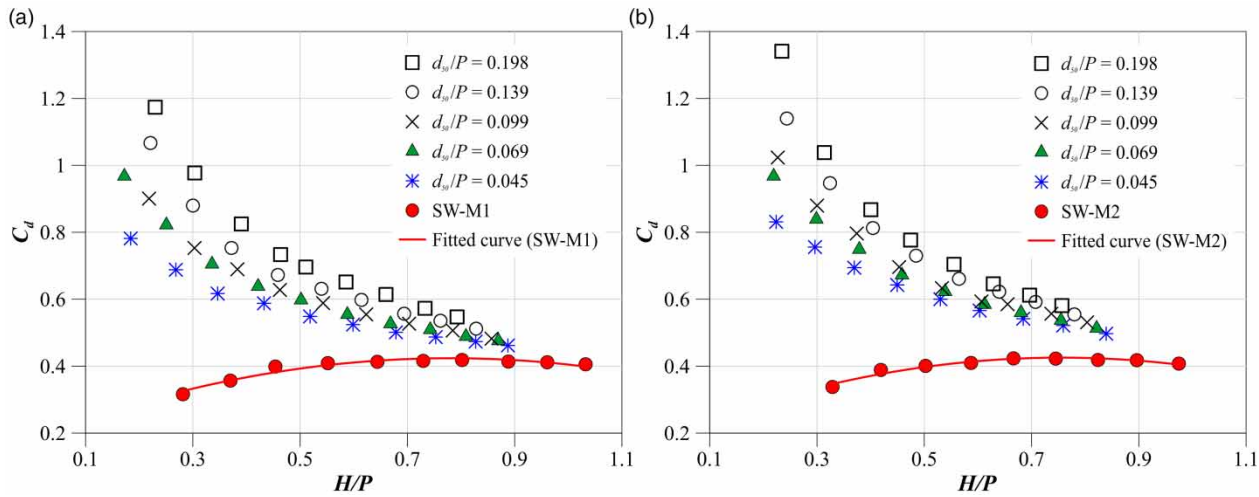

Figure 4 | Variation of C_d versus H/P for different filling material sizes compared with corresponding solid weir (a) PW-M1 and SW-M1 and (b) PW-M3 and SW-M2.

Hence, in low values of H/P ratios, less than 0.5, the discharge coefficient is significantly high due to the higher proportion of through flow to the total flow.

The discharge coefficients for different APPWs are presented in Figure 5. It can be inferred that in weirs with an arced-plan, increasing the weir's effective length increases the overflow and increases the weir's upstream contact surface; the through-flow fraction also increases. Thus, the maximum discharge coefficient belongs to the APPW with maximum effective length (PW-M2).

Threshold submergence boundary

Figure 6 shows the threshold submergence index Y_{TS} versus H/P for various ratios of d_{50}/P. There is a relatively linear correlation of the threshold submergence index with H/P. In this study, the threshold submergence index is defined purposefully as a function of the weir's height (P). According to this definition, if the threshold submergence occurs in a downstream depth lower/higher than the weir's crest level, then the threshold submergence index would be negative/positive, respectively. For example, if Y_{TS} is equal to -0.2 ($h_{TS} < P$) or 0.2 ($h_{TS} > P$), the threshold submergence occurs in a downstream depth of $0.2\,P$ lower or higher than the weir's crest level, respectively. For $Y_{TS} = 0$, the threshold submergence level is equal to the weir's height, P. Threshold submergence in the conventional impermeable weirs occurs at the stage in which the tailwater is higher than the weir's crest level (Hager & Schwalt 1994; Fritz & Hager 1998; Schmocker *et al.* 2011; Azimi *et al.* 2014). On the contrary, for most of the low discharge cases in this study, the threshold submergence occurred at the stage in which the downstream depth, h_d, was lower than the crest level of the porous weir. Results indicated that material sizes had no significant effect on the threshold submergence index.

The variation of threshold submergence index Y_{TS} versus H/P for different APPWs for two material sizes is illustrated in Figure 7. Results show that, for finer filling material, with the increases of weir's effective length in the arced-plan models, the threshold submergence index increases, and the APPW is less sensitive to downstream depth. Also, Figure 7(b) depicts that the threshold submergence index in all four weirs is not significantly different for the coarse filling material.

The DRF of submerged flow

Figure 8 shows the changes in the DRF versus relative submergence Γ for PW-M2 and PW-M4 for maximum (31.75 mm) and minimum (7.13 mm) filling material sizes. The relative submergence was defined as the $\Gamma = ((h_d/h_u) - (h_{TS}/h_u))/(1 - (h_{TS}/h_u))$, where $0 < \Gamma < 1$. Results show in both models that the DRF increases with an increase in the flow rate. In other words, with an increase in flow rate, the sensitivity of the APPW to the downstream depth decreases. However, for a high flow rate, the DRF is not significantly different.

Figure 9 compares the DRF values in each model for two different material sizes simultaneously with the corresponding solid weirs. Results show that with an increase in material size, the DRF coefficient decreases, and the weir is more prone

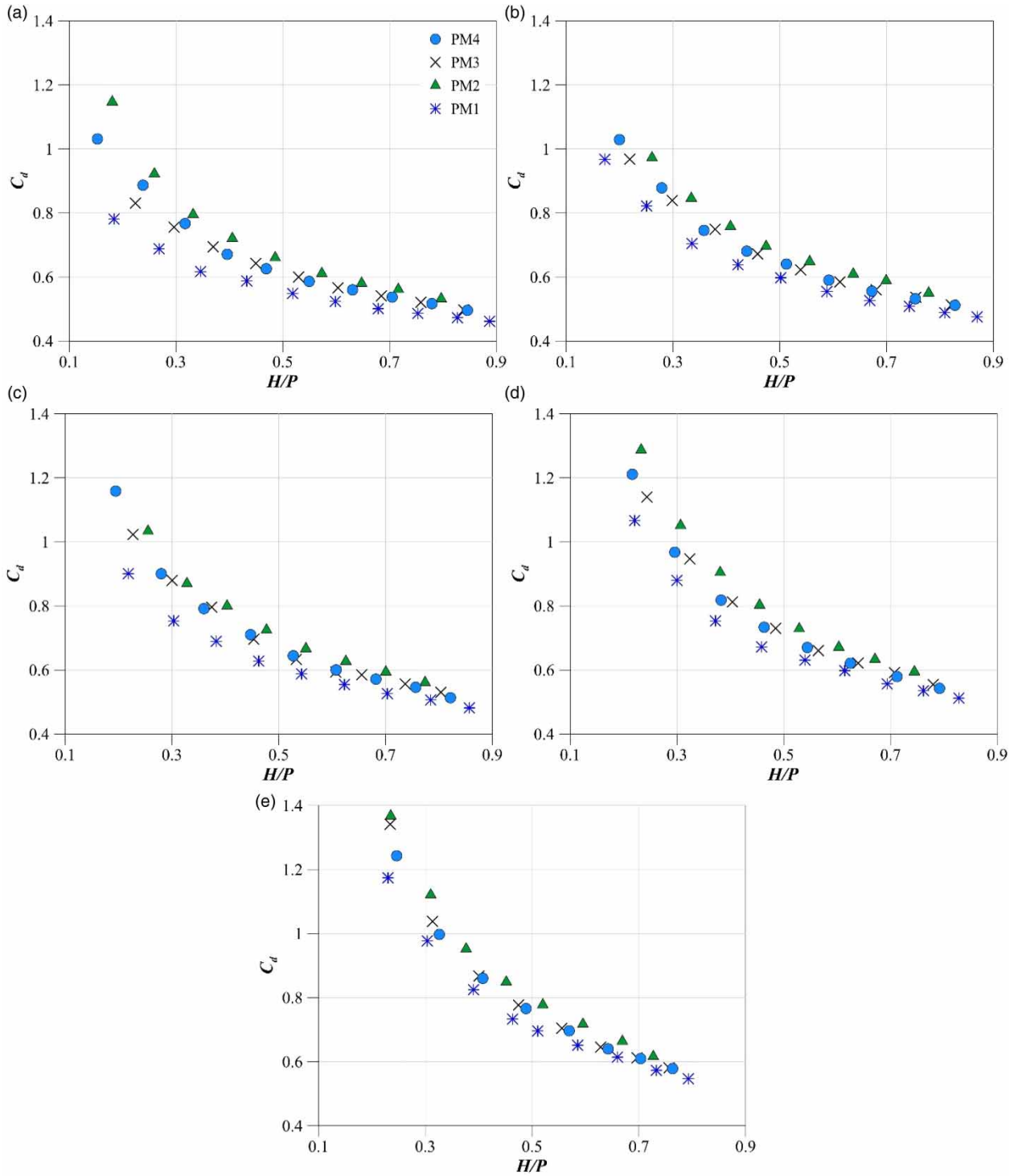

Figure 5 | Variation of C_d versus H/P for various APPWs.

to submergence. Comparing the porous and its corresponding solid weir results indicated that the impermeable weirs are less sensitive to downstream depths than porous weirs and are submerged at higher downstream depths.

Figure 10 shows the effect of different APPWs on DRF. For this purpose, the DRF values were compared in two different granulations for a constant flow rate. The results show that the weir's shape does not have a significant effect on the DRF.

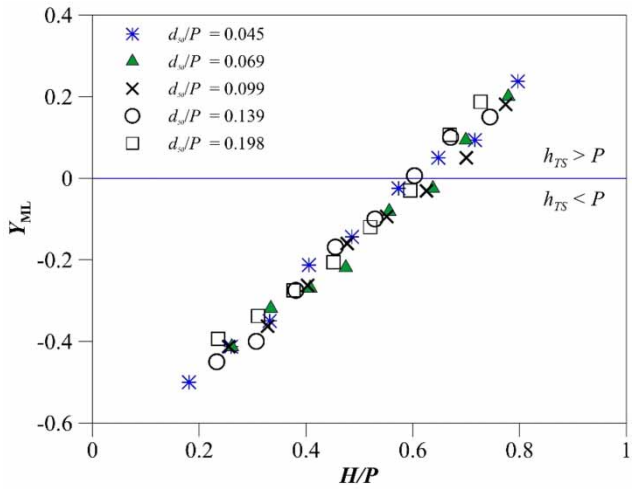

Figure 6 | Variation of Y_{TS} versus H/P for various d_{50}/P for PW-M2.

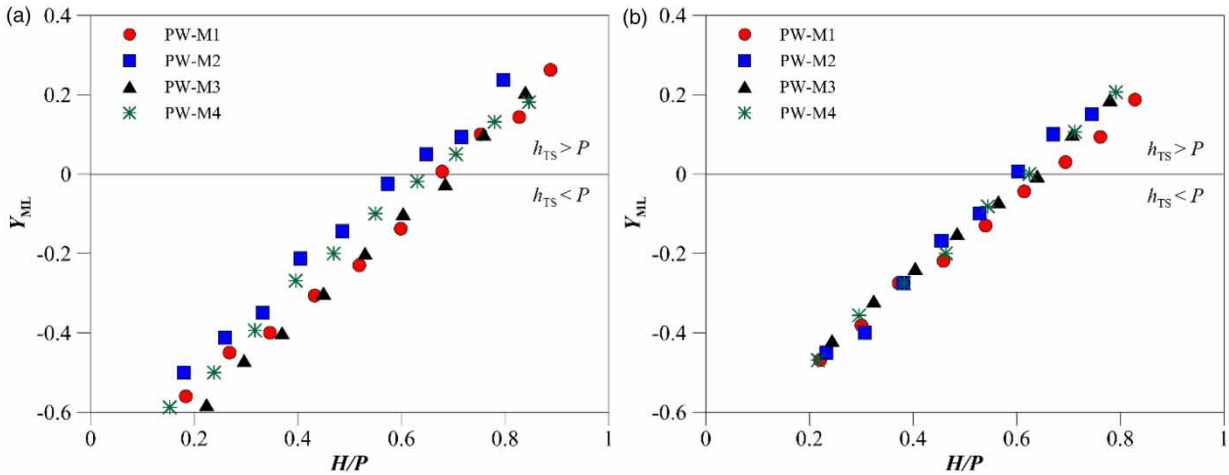

Figure 7 | Variation of Y_{TS} versus H/P for all APPWs for (a) $d_{50} = 7.13$ mm and (b) $d_{50} = 22.22$ mm.

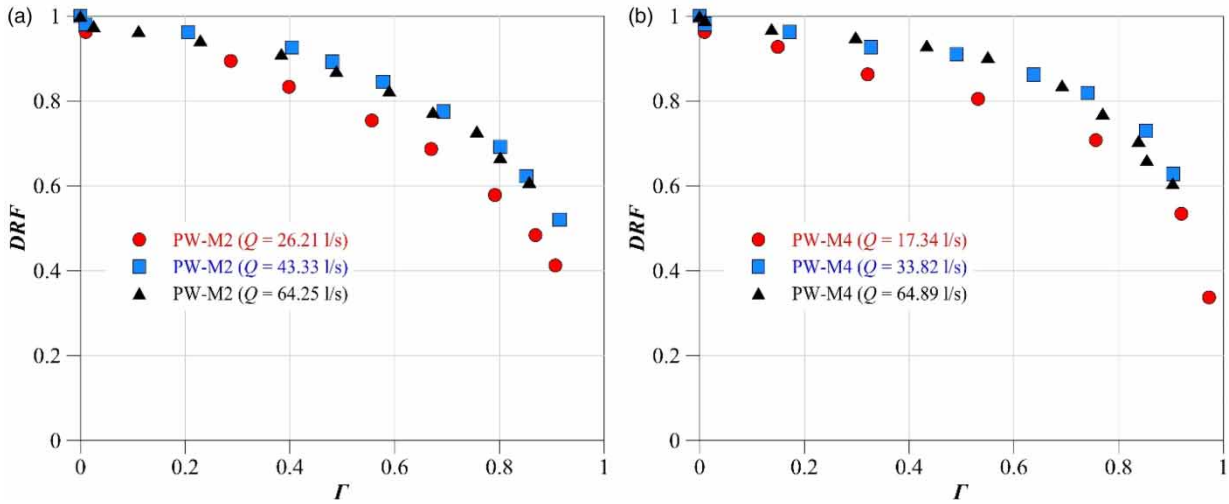

Figure 8 | Variations of DRF versus Γ for different flow rate in (a) PW-M2 ($d_{50}/P = 0.198$) and (b) PW-M4 ($d_{50}/P = 0.045$).

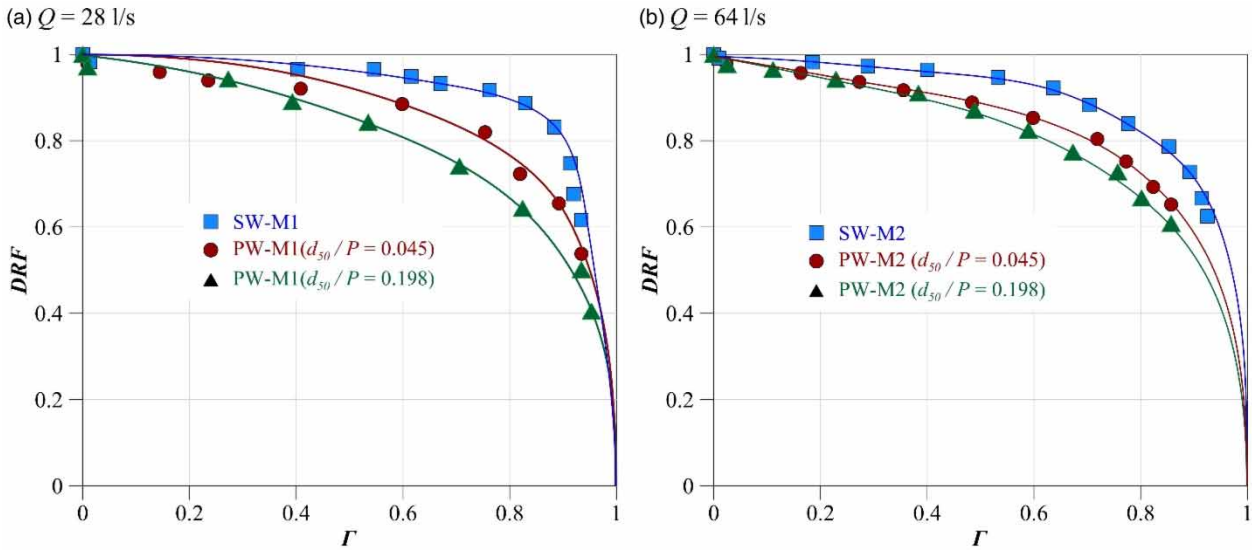

Figure 9 | Variations of DRF with submergence ratio for different d_{50}/P and comparison with the corresponding solid weirs.

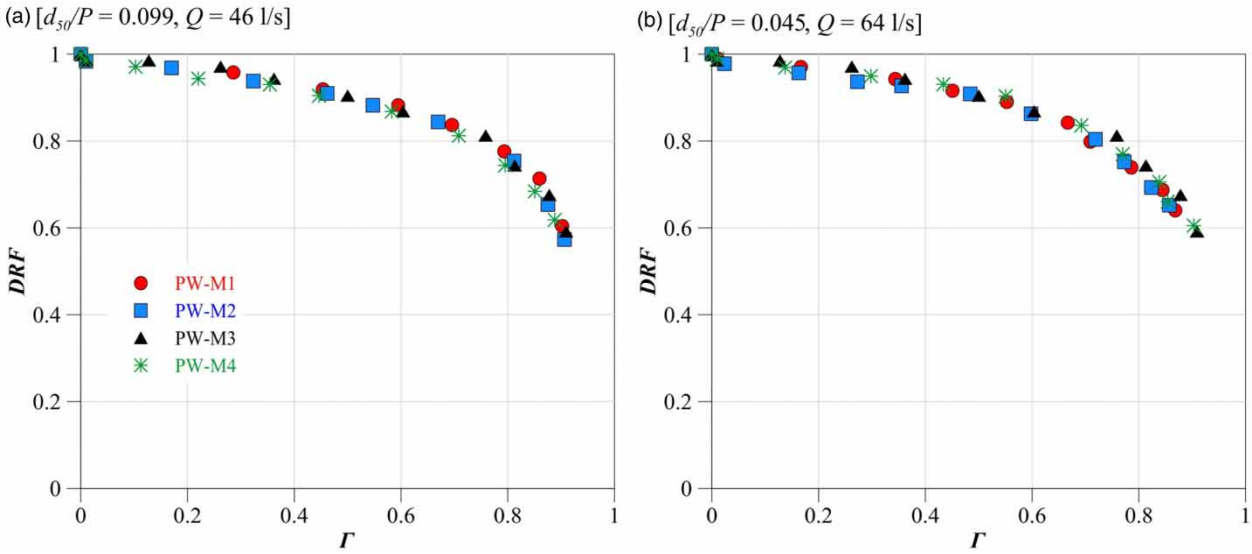

Figure 10 | Variations of DRF with submergence ratio for different APPWs.

Extraction of mathematical relationships

In this section, the aim is to extract the three relationships developed in the dimensional analysis section. To derive the free-flow discharge coefficient, threshold submergence index and submerged DRF, frequency relationships were first tested based on nonlinear multivariate regression using SPSS software. Considering that the user's selection of mathematical function type is performed at each step in a standard regression model, and the model determines only constant ratios, this method is very time-intensive. Further, it cannot be claimed that the best type of mathematical function is fitted due to the limitation of possible combinations of the selected mathematical functions. However, in soft computing models similar to GEP, the model intelligently selects both mathematical functions and constant ratios. Regarding the model's metaheuristic nature, the appropriate function is selected with a high speed (see Ferreira (2001a, 2001b) and Rahmanshahi & Shafai Bejestan (2020) for more details about GEP). It is noteworthy that d_{50}/P and $L_c//L_{Arc}$ were removed from Equations (8) and (9), respectively, because the dependence of the threshold submergence index on the particle size, as well as the DRF on the APPW shape, can be ignored. The optimal equations are developed as Equations (10)–(12). Also, in Figure 11, the observed and calculated

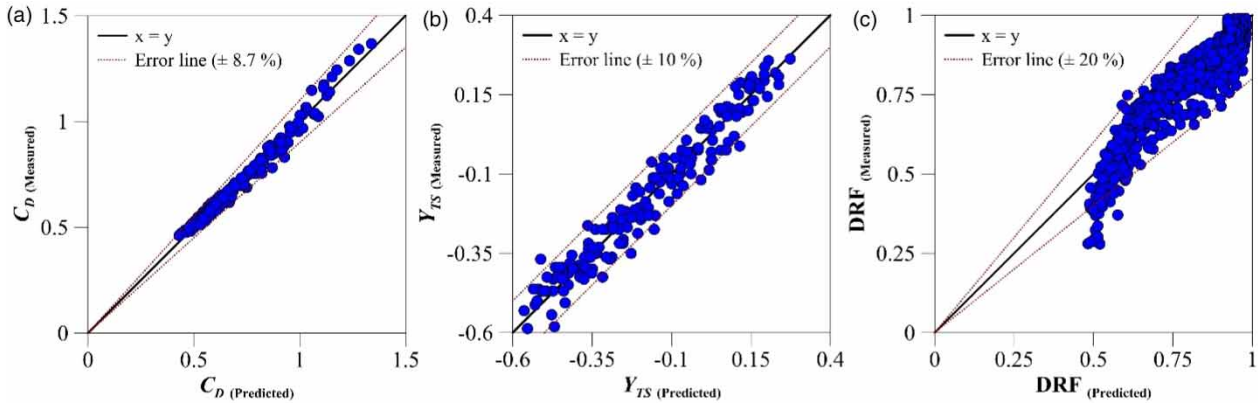

Figure 11 | Comparison of predicted and measured (a) free discharge coefficient, (b) threshold submergence index and (c) submerged DRF.

values are compared to the 45° line. The results show the appropriate accuracy of the fitted relationship. Statistical evaluation criteria, including the determination coefficient (R^2), the root mean square error (RMSE), and the mean absolute percentage error (MAPE) between the predicted and observed data, are displayed for each equation. The functional set and the rates assigned to operational parameters used in GEP modelling are listed in Table 3.

$$C_d = n/\left(n + \frac{H - d_{50}}{P} + \frac{L_c}{L_{Arc}} - 0.31\right) - 0.22\,(n-1)\frac{H}{nP} - \frac{L_c}{L_{Arc}} \tag{10}$$

$[R^2 = 0.98,\ RMSE = 0.026,\ MAPE = 0.026]$

$$Y_{TS} = \left(\frac{H}{P} - \frac{L_c}{L_{Arc}} - 1.97\right) \Big/ \left(n - \frac{H}{P} + 2.38\right) + \frac{H}{P} \tag{11}$$

$[R^2 = 0.95,\ RMSE = 0.05,\ MAPE = -0.009]$

$$DRF = \frac{1}{2}\left(\Gamma + \frac{d_{50}}{P}\right)\left(\Gamma^2 - \frac{d_{50}}{P}\right) - \frac{d_{50}}{2P} + 1 \tag{12}$$

$[R^2 = 0.91,\ RMSE = 0.044,\ MAPE = 0.041]$

APPW direction effects

This section compares the hydraulic performances of two types of APPWs with the same geometry but in the opposite direction. For this purpose, PW-M3 with the same grain size in two different directions was tested according to Figure 12(a) and

Table 3 | Parameters of the optimized GEP model

Parameters	Setting of parameter
Function set	+, −, /, ×
Population size	30
Number of gene	1
Mutation rate	0.025
Inversion rate	0.1
One-point recombination rate	0.3
Two-point recombination rate	0.3
Gene recombination rate	0.1
Gene transposition rate	0.1

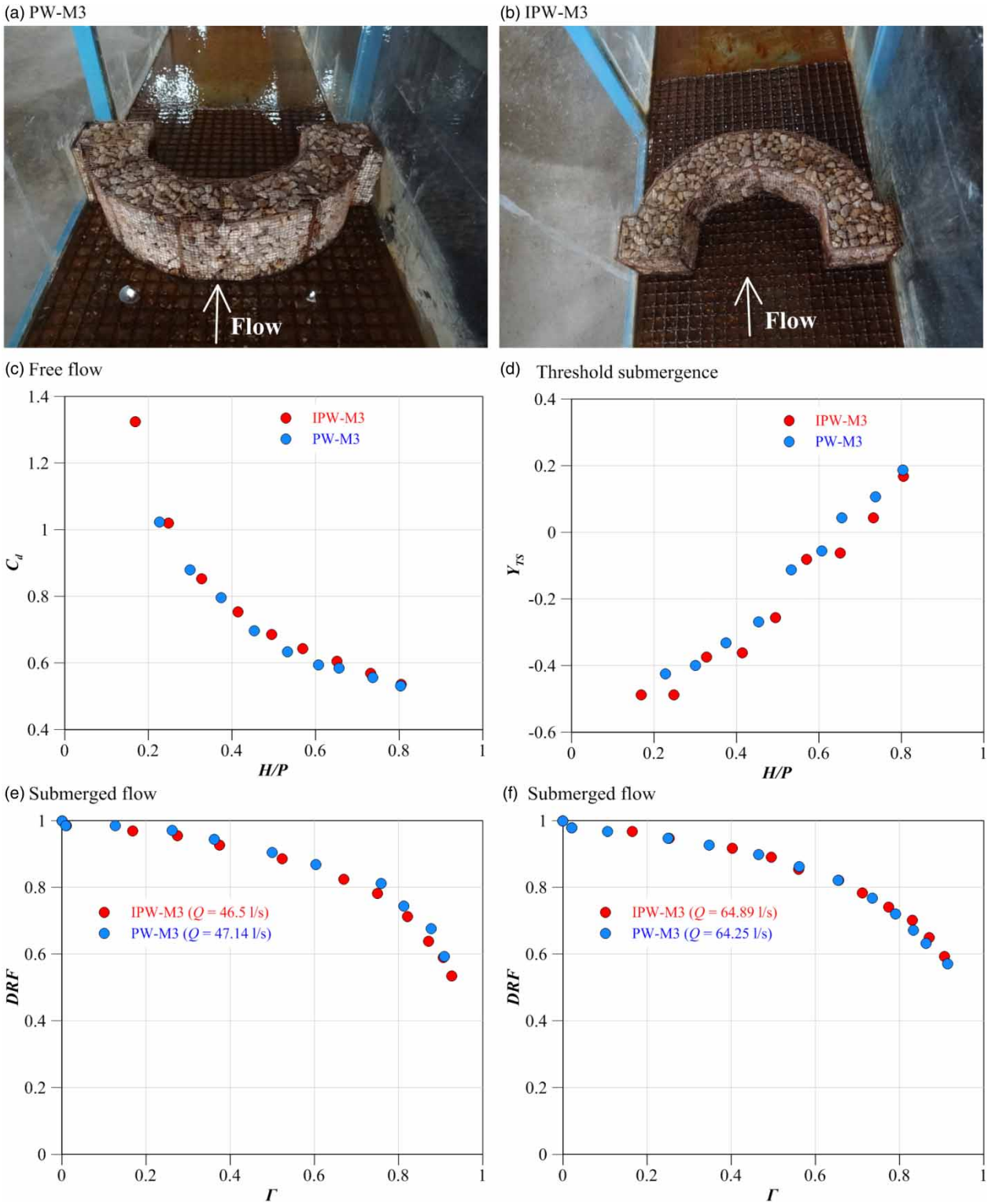

Figure 12 | Comparison of C_d, Y_{TS} and DRF for PW-M3 versus IPW-M3, (a) PW-M3 experiment model, (b) IPW-M3 experiment model, (c) C_d, (d) Y_{TS}, and (e,f) DRF.

12(b). In Figure 12(c), the free discharge coefficient and Figure 12(d), the threshold submergence index of these two models are compared. The results show that there is no significant difference between these two weirs. Figure 12(e) and 12(f) depicts their DRF for two different flow rates. The results indicated that for a specific discharge, DRF is almost the same for both

weirs. Hence, it can be concluded that for similar material size and flow rate, the effects of APPWs direction do not affect the hydraulic performance of the weir in both free and submerged flow conditions.

CONCLUSIONS

In this study, an experimental investigation was performed to determine the free discharge coefficient, threshold submergence and submerged DRF of APPWs in different geometric and hydraulic conditions. In free-flow conditions, the water surface profile downstream of the APPWs has a convexity in the channel's centreline that increases with increasing flow rate. Like other weirs, the weir's downstream water surface in the submerged conditions has surface waves that decrease with increasing submergence ratio. The submerged discharge coefficient can be 68% less than the corresponding free-flow discharge coefficient. Results show that with increasing material sizes, the discharge coefficient increases. Unlike solid weirs, the discharge coefficient decreases with increasing H/P (or discharge) ratio in porous weirs. The difference between C_d of different particle sizes is reduced with increasing H/P and for H/P values greater than 0.9, and the discharge coefficient values of solid and porous weirs are very close to each other. It can be inferred that in weirs with an arced-plan, increasing the weir's effective length increases the discharge coefficient. The threshold submergence of porous weirs occurred at the stage in which the downstream depth was lower than the weir's crest. Results indicated that material sizes had no significant effect on the threshold submergence index. For finer filling material, with an increase in the effective length of the weir, the threshold submergence index of APPWs increases and it is not significantly different for the coarse filling material. The DRF increases with an increase in the flow rate, and for a high flow rate, the DRF is not significantly different. The DRF coefficient decreases with an increase in material sizes. The weir's shape does not have a significant effect on the DRF. Hence, it can be concluded that for similar material size and flow rate, the effects of APPWs direction do not affect the hydraulic performance of the weir in both free and submerged flow conditions. Finally, three mathematical relationships were developed to estimate the free discharge coefficient, the threshold submergence index and the submerged DRF.

ACKNOWLEDGEMENTS

The authors would like to acknowledge the Islamic Azad University Shoushtar Branch and Khuzestan Water and Power Authority (KWPA) for financial support and facilitation of the experiments.

DATA AVAILABILITY STATEMENT

All relevant data are included in the paper or its Supplementary Information.

REFERENCES

Azimi, A. H., Rajaratnam, N. & Zhu, D. Z. 2014 Submerged flows over rectangular weirs of finite crest length. *Journal of Irrigation and Drainage Engineering* **140** (5), 06014001. https://doi.org/10.1061/(ASCE)IR.1943-4774.0000728.

Barenblatt, G. I. 1987 *Dimensional Analysis*. Gordon and Breach, Science Publishers, Amsterdam.

Chanson, H. 2006 Discussion of discharge through a permeable rubble mound weir. *Journal of Hydraulic Engineering* **132** (4), 432–434.

Crookston, B. M. & Tullis, B. P. 2012 Arced labyrinth weirs. *Journal of Hydraulic Engineering* **138** (6), 55. https://doi.org/10.1061/(ASCE)HY.1943-7900.0000553.

Fathi-moghadam, M., Tavakol Sadrabadi, M. & Rahmanshahi, M. 2018 Numerical simulation of the hydraulic performance of triangular and trapezoidal gabion weirs in free flow condition. *Flow Measurement and Instrumentation* **62** (2018), 93–104. https://doi.org/10.1016/j.flowmeasinst.2018.05.005.

Ferreira, C. 2001a Gene expression programming in problem solving. In: *Proceedings of the 6th Online World Conference on Soft Computing in Industrial Applications*. pp. 635–653.

Ferreira, C. 2001b Gene expression programming: a new adaptive algorithm for solving problems. *Complex Systems* **13** (2), 87–129.

Fritz, H. M. & Hager, W. H. 1998 Hydraulics of embankment weirs. *Journal of Hydraulic Engineering* **124** (9), 963–971. https://doi.org/10.1061/(ASCE)0733-9429(1998)124:9(963).

Hager, W. & Schwalt, M. 1994 Broad crested weir. *Journal of Irrigation and Drainage Engineering* **120** (1), 13–26. https://doi.org/10.1061/(ASCE)0733-9437(1994)120:1(13).

Horton, R. E. 1907 *Weir Experiments, Coefficients, and Formulas. Proceedings of the U.S. Geological Survey Water Supply*. Government Printing Office, Washington, DC. https://doi.org/10.1061/(ASCE)0733-9429(2005)131:1(1).

Kells, J. A. 1993 Spatially varied flow over rockfill embankments. *Canadian Journal of Civil Engineering* **20** (5), 820–827. https://doi.org/10.1139/l93-107.

Kells, J. A. 1994 Reply on discussion of spatially varied flow over rockfill embankments. *Canadian Journal of Civil Engineering* **21** (1), 163–166. https://doi.org/10.1139/l94-016.

Leu, J. M., Chan, H. C. & Chu, M. S. 2008 Comparison of turbulent flow over solid and porous structures mounted on the bottom of a rectangular channel. *Flow Measurement and Instrumentation* **19** (6), 331–337. https://doi.org/10.1016/j.flowmeasinst.2008.05.001.

Michioku, K., Maeno, S., Furusawa, T. & Haneda, M. 2005 Discharge through a permeable rubble mound weir. *Journal of Hydraulic Engineering* **131** (1), 1–10.

Michioku, K., Takehara, K. & Etoh, T. 2007 An experimental study on flow field in and around rubble mound river structures. *Journal of Hydraulic Engineering* **25** (2), 37–45.

Mohamed, H. 2010 Flow over gabion weirs. *Journal of Irrigation and Drainage Engineering* **136** (8), 573–577. https://doi.org/10.1061/(ASCE)IR.1943-4774.0000215.

Mohammadpour, R., Ghani, A. A. & Azamathulla, H. M. 2013 Numerical modeling of 3-D flow on porous broad crested weirs. *Applied Mathematical Modelling* **37** (22), 9324–9337. https://doi.org/10.1016/j.apm.2013.04.041.

Novak, P. & Cabelka, J. 1981 *Models in Hydraulic Engineering*. Pitman, London, UK.

Rahmanshahi, M. & Shafai Bejestan, M. 2020 Gene-expression programming approach for development of a mathematical model of energy dissipation on block ramps. *Journal of Irrigation and Drainage Engineering* **146** (2), 04019033. https://doi.org/10.1061/(ASCE)IR.1943-4774.0001442.

Safarzadeh, A. & Mohajeri, S. H. 2018 Hydrodynamics of rectangular broad-crested porous weirs. *Journal of Irrigation and Drainage Engineering* **144** (10), 04018028. https://doi.org/10.1061/(ASCE)IR.1943-4774.0001338.

Salmasi, F. & Taghi Sattari, M. 2017 Predicting discharge coefficient of rectangular broad-crested gabion weir using M5 tree model. *Iranian Journal of Science and Technology, Transactions of Civil Engineering* **41** (2), 205–2012. https://doi.org/10.1007/s40996-017-0052-5.

Salmasi, F., Sabahi, N. & Abraham, J. 2021 Discharge coefficients for rectangular broad-crested gabion weirs: experimental study. *Journal of Irrigation and Drainage Engineering* **147** (3), 04021001. https://doi.org/10.1061/(ASCE)IR.1943-4774.0001535.

Schmocker, L., Halldórsdóttir, B. & Hager, W. 2011 Effect of weir face angles on circular-crested weir flow. *Journal of Hydraulic Engineering* **137** (6), 637–643. https://doi.org/10.1061/(ASCE)HY.1943-7900.0000346.

Shariq, A., Hussain, A. & Ahmad, Z. 2020 Discharge equation for the gabion weir under through flow condition. *Flow Measurement and Instrumentation* **74**, 101769. https://doi.org/10.1016/j.flowmeasinst.2020.101769.

First received 3 September 2021; accepted in revised form 9 December 2021. Available online 23 December 2021